DOI: 10.31276/VJSTE.2026.0044 *Physical Sciences* | *Chemistry; Engineering*

Fluorine-free superhydrophobic steel mesh prepared by ZnO electrodeposition and MTES modification for effective oil-water separation

Nguyen Thi Phuong Nhung*, Vo Chi Hao

PetroVietnam University, 762 Cach Mang Thang Tam Street, Ba Ria Ward, Ho Chi Minh City, Vietnam

Received 9 June 2026; revised 7 September 2026; accepted 12 September 2026

Abstract:

The development of environmentally friendly superhydrophobic materials for oil-water separation remains a significant challenge. In this study, a fluorine-free superhydrophobic/superoleophilic stainless steel mesh was fabricated by ZnO electrodeposition followed by methyltriethoxysilane (MTES) modification. The hierarchical ZnO micro/nanostructures combined with the low-surface-energy MTES layer produced water contact angles above 150°. The modified mesh enabled gravity-driven separation of condensate oil/water mixtures, achieving a mean separation efficiency of 95.7±2.5% (n=10) and a representative permeation flux of 7.82×10^{3} $L\cdot m^{-2}\cdot h^{-1}$. The mesh remained functional over ten consecutive reuse cycles and retained its superhydrophobic/superoleophilic characteristics after six months of ambient storage, indicating good short-term reusability and storage stability. These results demonstrate that ZnO electrodeposition combined with fluorine-free MTES modification provides a simple and effective strategy for fabricating superhydrophobic stainless steel meshes for gravity-driven separation of immiscible oil/water mixtures.

Keywords: **micro/nanostructured ZnO layer, oil/water separation, superhydrophobic.**

Classification numbers: **2.2, 2.3**

*Corresponding author: Email: nhungntp@pvu.edu.vn; nguyenphuongnhungvn@gmail.com

1. Introduction

Environmental pollution caused by industrial oily wastewater, marine oil spills, and domestic discharge has become a serious threat to ecosystems and human health. Conventional oil-water separation techniques, such as sedimentation, coagulation, and flotation, have been widely applied; however, they often suffer from low efficiency, high operational costs, and the risk of secondary pollution [1]. In recent years, advances in materials science have enabled the development of special wettability materials, particularly superhydrophobic and superoleophilic surfaces, which have demonstrated promising performance in oil-water separation applications [2]. These materials can selectively allow oil to pass through while repelling water, or vice versa, depending on their designed surface wettability. They have been fabricated on a variety of supports, including textiles [3], sponges [4], aerogels [5], and metallic structures [1].

Although sponges and aerogels exhibit high oil absorption capacity, their practical application is limited by poor mechanical durability and vulnerability to repeated mechanical and chemical stresses [6]. In addition, regeneration processes are often energy intensive because oil can deeply penetrate into their three-dimensional porous networks [7]. Textile-based systems offer advantages such as low cost, flexibility, and lightweight properties; however, they typically suffer from limited stability under harsh conditions. Moreover, functional coatings may be damaged during repeated use, reducing the long-term stability of the material. Furthermore, these materials are often more suitable for simple immiscible mixtures and may be difficult to implement in continuous flow or long-term separation systems [8].

In recent years, considerable efforts have been devoted to developing fluorine-free and bioinspired superhydrophobic materials to further improve the sustainability, mechanical robustness, and multifunctionality of oil/water separation systems. Biobased cotton fabrics fabricated via impregnation or dip coating methods

have demonstrated excellent superhydrophobicity, flame retardancy, chemical stability, and reusability for treating oily wastewater [9-13]. Biomimetic superhydrophobic sponges incorporating magnetic or multifunctional components have also been developed to enable multi-path oil recovery, including magnetically driven, gravity-driven, and photothermally driven separation modes [14, 15]. These studies collectively highlight an emerging trend towards eco-friendly, fluorine-free, and multifunctional superhydrophobic materials, which further motivates the development of durable and scalable metal-mesh-based alternatives, such as the ZnO/methyltriethoxysilane (MTES)-modified stainless steel mesh reported in this work.

In contrast, metallic frameworks, particularly stainless steel meshes, provide several advantages for oil-water separation. Metal mesh substrates possess high mechanical strength, thermal stability, corrosion resistance, and well-defined pore structures, which are beneficial for continuous gravity-driven separation systems. In addition, their pore size and surface wettability can be adjusted to control separation performance. Compared with sponges, fabrics, and polymer-based membranes, stainless steel meshes are more robust and can be readily modified by chemical or electrochemical methods to construct functional surfaces with improved adhesion and durability [16]. Recent studies have also shown that metal-mesh-based special wettability materials are promising for practical oil-water separation due to their high separation efficiency, reusability, self-cleaning behaviour, and potential multifunctionality. For example, superhydrophobic magnetic nickel nanowires grafted with a silane coupling agent [17] and superhydrophobic/superoleophilic micro/nanostructured nickel particles [18] have demonstrated high separation efficiency and good reusability for both simple oil/water mixtures and surfactant-stabilised emulsions, further confirming the strong potential of metal-based superhydrophobic materials, including metal meshes, for practical oil-water separation.

The fabrication of superhydrophobic materials typically relies on two key factors: the construction of micro/nanoscale roughness and the introduction of low-surface-energy chemical groups [1, 16, 19]. The surface roughness can amplify the intrinsic wettability of a material and promote the formation of air pockets between the water droplet and the solid surface, leading to a Cassie-Baxter wetting state. Therefore, surface microstructure and chemical composition are both essential for achieving stable superhydrophobicity. As summarised in Table 1, hierarchical surface structures can be produced through either top-down or bottom-up approaches. Top-down strategies involve material removal processes, including photolithography, chemical etching, laser ablation, and mechanical polishing. In contrast, bottom-up methods rely on the growth or assembly of nanostructures through techniques such as hydrothermal synthesis, sol-gel processing, chemical vapour deposition (CVD), electrodeposition, and various coating approaches.

Table 1. Comparison of representative superhydrophobic mesh materials for oil-water separation.

References	Roughness fabrication method	Surface modification method/agent	WCA (°)	Separation efficiency (%)
[20]	Spray coating with NS/melamine-urea-formaldehyde resin	Octadecyl acrylate (ODA)	>160	>98
[21]	Heterogeneous nucleation via immersion in alcoholic zinc acetate dihydrate/diethanolamine solution	Stearic acid (STA)	162	99
[22]	SiO2 nanoparticle dip-coating	Polystyrene layering	158	>87
[23]	ZnO/Zn-Ni electrodeposition	PFOTS in ethanol	—	97.3
[24]	Polystyrene coating	OTS	157.5	>89
[25]	Ni-WS2 electrodeposition	WS2	169	>98

Among these methods, electrodeposition is attractive for modifying metallic substrates because it is relatively simple, controllable, and suitable for forming micro/nanostructured coatings directly on conductive surfaces. Compared with some physical techniques that require expensive equipment or harsh processing conditions, electrodeposition can be performed under mild conditions and allows the surface morphology to be tuned by adjusting the deposition parameters. For stainless steel meshes, this method is particularly useful because the conductive framework can serve directly as the electrode, enabling the formation of rough inorganic layers with good surface coverage.

To reduce surface energy, chemical modification is commonly performed using fatty acids, silanes, or polymer-based agents [1, 26, 27]. Fluorinated compounds are frequently employed because of their excellent hydrophobic properties; however, increasing concerns regarding their environmental persistence and potential health impacts have motivated the development of fluorine-free alternatives. In addition, some polymer-based coatings often require multiple processing steps to achieve the desired surface wettability and durability. Therefore, developing a simple, scalable, and fluorine-free strategy for fabricating superhydrophobic stainless steel meshes remains important for practical oil-water separation.

Despite this progress, most previously reported ZnO-based superhydrophobic meshes rely on hydrothermal growth, chemical bath deposition, or spray coating combined with fluorinated silanes to achieve low surface energy [20, 23]. Electrodeposition offers a faster and more controllable alternative for building ZnO micro/nanostructures directly on conductive mesh substrates, yet studies that systematically correlate ZnO electrodeposition time with surface wettability, and that pair this process with a fluorine-free modifier, remain scarce. Consequently, a clear understanding of how electrodeposition duration governs the roughness-wettability relationship, and whether a fluorine-free coating can still deliver durable, chemically stable superhydrophobicity, is still lacking. Notably, our research group has

previously demonstrated the successful application of ZnO-based micro/nanostructuring for constructing superhydrophobic steel surfaces with enhanced corrosion resistance [2], confirming the feasibility and reproducibility of this fabrication approach on steel substrates. Building on this foundation, the present study extends the ZnO electrodeposition strategy, combined with a fluorine-free MTES modification, to stainless steel mesh for gravity-driven oil-water separation.

In this context, the present study aims to fabricate a fluorine-free superhydrophobic/superoleophilic stainless steel mesh for efficient oil-water separation. A hierarchical micro/nanostructured ZnO layer was constructed on the mesh via mild electrodeposition, followed by modification with MTES, a fluorine-free silane. The ZnO layer provides the hierarchical roughness required for superhydrophobicity, while MTES grafts low-surface-energy methyl groups to enhance water repellency. The effect of ZnO electrodeposition time on wettability was systematically investigated, and the morphology, composition, chemical stability, and separation performance of the modified mesh were evaluated, offering a facile, fluorine-free route to durable superhydrophobic meshes.

The novelty of this work lies in combining hierarchical ZnO structures produced by electrodeposition with fluorine-free MTES modification for gravity-driven oil/water separation. In addition, the effect of electrodeposition time on surface wettability was systematically evaluated, with SEM observations providing qualitative morphological support. The resulting mesh also exhibited chemical stability over pH 1-13, short-term reusability over ten cycles, and six-month ambient storage stability.

2. Materials and methods

2.1. Materials

MTES, ethanol, zinc acetate, sodium chloride, copper sulphate, and hydrochloric acid (HCl) were purchased from Xilong (China). Stainless steel mesh (wire diameter ~75 µm, pore size 85-175 µm) was used as the substrate. A zinc plate

was used as the anode during electrodeposition. Deionised water was used throughout all experiments. All chemicals were used as received without further purification.

2.2. Preparation of superhydrophobic surface

The fabrication procedure of the superhydrophobic mesh is schematically illustrated in Fig. 1. Pristine stainless steel mesh was cut into 3×3 cm pieces and cleaned by ultrasonication in ethanol for 5 min, followed by rinsing with deionised water and drying under ambient conditions. Prior to electrodeposition, the cleaned mesh was immersed in 0.1 M HCl for 30 s to remove the native oxide layer. The cleaned mesh was subsequently converted into a ZnO-coated mesh via electrodeposition in a two-electrode electrochemical cell, using a zinc plate as the anode and the stainless steel mesh as the cathode. The electrolyte consisted of 0.1 M zinc acetate ($Zn(CH_3COO)_2$) and 0.1 M NaCl dissolved in approximately 250 ml of deionised water, and the two electrodes were positioned parallel to each other at a fixed distance of ~8 cm. Electrodeposition was carried out under continuous magnetic stirring at a constant applied voltage of 0.9 V (measured current of ~0.4 mA) for 10, 15, 20, 25, 30, 35, 40, and 45 min. This voltage was selected on the basis of our previously reported electrodeposition protocol, which was successfully applied to construct hierarchical ZnO micro/nanostructures on stainless steel substrates, providing a suitable balance between deposition rate and coating uniformity while avoiding the excessive crystal growth observed at higher voltages [2]. After electrodeposition, the ZnO-coated mesh was thoroughly rinsed with deionised water and dried in air. Finally, the ZnO-coated mesh was rendered superhydrophobic through surface modification with MTES. The mesh was first treated with UV/ozone for 15 min on each side, with a 5 min interval between treatments, to generate surface hydroxyl groups. It was then immersed in a 10 vol% MTES solution in ethanol and heated in a sealed glass vessel at 60-70°C overnight, during which MTES underwent hydrolysis to form silanol groups that subsequently

underwent condensation with hydroxylated surface sites, forming a low-surface-energy MTES-derived silane layer. The resulting superhydrophobic mesh was rinsed three times with ethanol and dried under ambient conditions. Unless otherwise specified, all experiments were performed under laboratory ambient conditions.

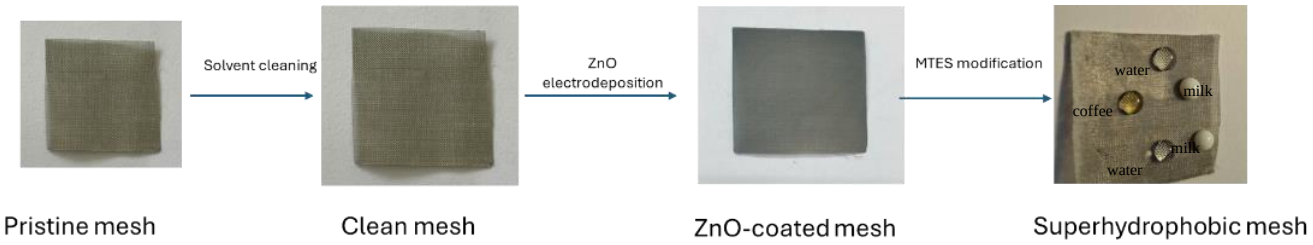


Fig. 1. Schematic of the fabrication process for a superhydrophobic mesh. Source: Made by the authors.

2.3. Surface analyses

The surface morphology and elemental composition were characterised using scanning electron microscopy equipped with energy-dispersive X-ray spectroscopy (SEM-EDS, JEOL 7600F, Oxford Instruments, the United Kingdom). The wettability of the samples was evaluated by measuring the static water contact angle using a contact angle goniometer (OCA, DataPhysics, Germany). Measurements were performed at three different positions on each sample using 5 µl distilled water droplets.

2.4. Oil/water separation test

To evaluate the oil/water separation performance of the fabricated superhydrophobic/superoleophilic (SHB/SOL) mesh, the mesh was fixed onto the perforated cap of a plastic tube with an inner diameter of 1.5 cm, and the cap was tightly screwed onto the tube to secure the mesh in place; the opposite end of the tube was left open, forming a simple gravity-driven separation apparatus (Fig. 2).

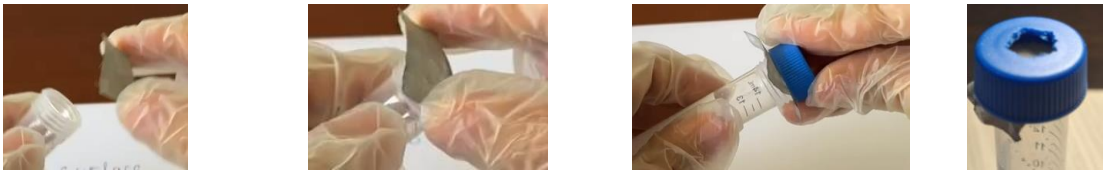


Fig. 2. The loading process of the modified mesh into a tubular separation device. Source: Made by the authors.

A stratified mixture consisting of equal volumes of condensate oil and $CuSO_4$-dyed water (total volume of 40 ml) was introduced into the apparatus, and the oil phase was allowed to permeate through the mesh under gravity while the water phase was retained above the surface (Fig. 3).

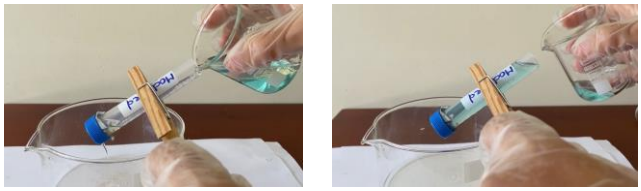


Fig. 3. The separation of oil/water mixtures using a superhydrophobic mesh. Source: Made by the authors.

The volume of permeated oil and the separation time were recorded for each test. The oil/water separation efficiency (η) and the permeation flux (F) were calculated according to Equations (1) and (2), respectively:

$$\eta\ (\%) = (V_{oil,\ permeated} / V_{oil,\ initial}) \times 100\% \quad (1)$$

$$F = V/(S \times t) \quad (2)$$

where $V_{oil,\ permeated}$ is the volume of oil collected after separation; $V_{oil,\ initial}$ is the initial volume of oil in the mixture; V is the volume of permeated oil; S is the effective separation area of the mesh; and t is the separation time. After each separation test, the mesh was rinsed with ethanol and dried before reuse.

3. Results and discussion

3.1. Surface wettability, morphology, and chemical composition analysis

In this section, the surface wettability was tuned by varying the ZnO electrodeposition time. Fig. 4 presents the corresponding water contact angles for mesh surfaces prepared under different deposition durations.

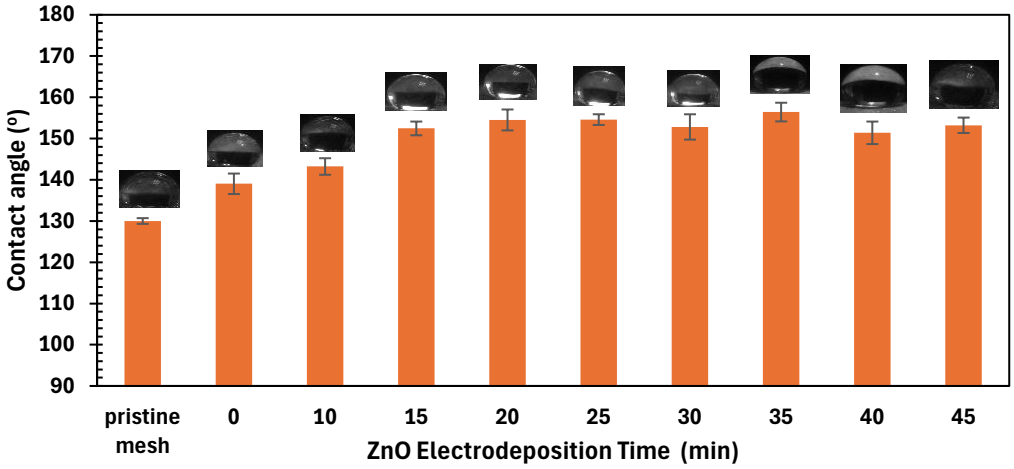


Fig. 4. Wettability of the modified mesh surface as a function of ZnO electrodeposition time. Source: Made by the authors.

The pristine mesh exhibited hydrophobic behaviour with a contact angle of approximately 130°, although the water droplet remained pinned to the surface, indicating high contact angle hysteresis. This elevated apparent contact angle, compared to flat stainless steel (typically 60-90°), is attributed to the geometry of the woven mesh rather than its intrinsic surface chemistry: the cylindrical wires provide a re-entrant-like microtexture at crossover points, and the mesh porosity allows partial air entrapment beneath the droplet. The accompanying high contact angle hysteresis indicates a Wenzel-like or mixed wetting state, consistent with partial liquid penetration into the mesh interstices. Comparable apparent contact angles have been reported for other pristine, uncoated stainless steel meshes [28]. After modification with MTES alone, the mesh became more hydrophobic but did not reach the superhydrophobic regime (WCA≥150°). In contrast, the ZnO/MTES-modified meshes exhibited superhydrophobicity at electrodeposition times of 15 min

or longer (≥15 min), with the highest water contact angles observed within the 20-35 min range. This behaviour is attributed to the hierarchical ZnO micro/nanostructures, which, together with the low-surface-energy MTES layer, promote air entrapment and a Cassie-Baxter wetting state. At shorter deposition times (<15 min), the lower contact angles suggest that the developed surface structure was not sufficient to sustain effective air entrapment. Beyond 35 min, the slight decrease in contact angle may result from excessive ZnO growth and structural coarsening, which could reduce effective air retention and increase liquid-solid contact. Because coating thickness and time-resolved surface morphology were not quantitatively measured, this explanation is proposed as a plausible mechanism rather than a definitive conclusion.

Fig. 5 compares the wetting behaviour of the pristine mesh and the superhydrophobic mesh.

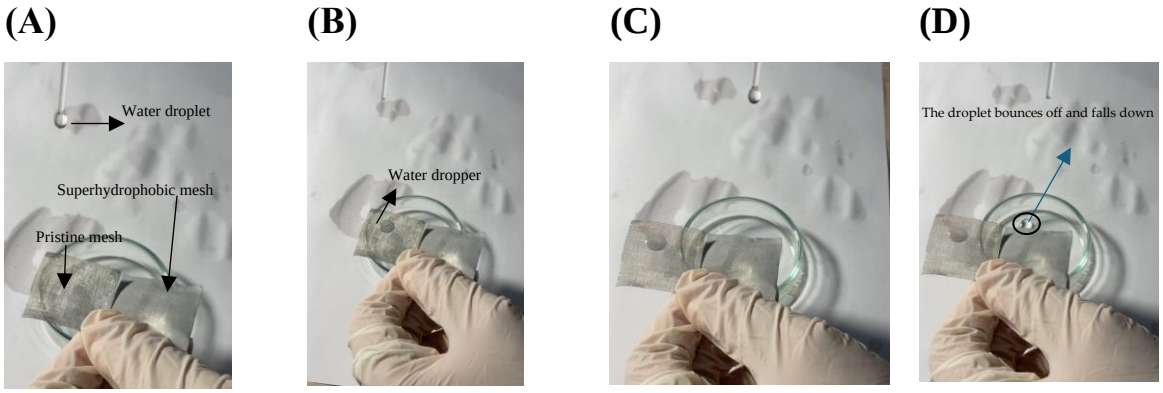


Fig. 5. Optical images of water droplet deposition on two surfaces: the pristine mesh (left) and the superhydrophobic mesh (right). (A) Before deposition on the pristine mesh; **(B)** After deposition on the pristine mesh surface; **(C)** Before deposition on the superhydrophobic mesh; **(D)** After deposition on the superhydrophobic surface. Source: Made by the authors.

When a water droplet is released onto the pristine mesh surface (Figs. 5A-5B), it adheres strongly and remains pinned, indicating high contact angle hysteresis. In contrast, under identical conditions, a droplet impacting the superhydrophobic

surface rebounds and detaches from the surface (Figs. 5C-5D), demonstrating low adhesion and high water repellency. This distinct wetting behaviour can be attributed to the combined effects of surface roughness and surface energy modification. The ZnO coating introduces hierarchical micro/nanostructures on the mesh surface, increasing surface roughness compared to the pristine substrate. Meanwhile, MTES modification reduces the surface energy through the introduction of hydrophobic -CH_3 groups during the silanisation process. The synergistic effect of these two factors promotes the formation of a Cassie-Baxter wetting state, in which air pockets are trapped within the surface structures. As a result, the contact area between the water droplet and the solid surface is significantly reduced, leading to low adhesion and droplet rebound behaviour.

Fig. 6 presents SEM images of the pristine mesh (Figs. 6A-6C) and the superhydrophobic mesh (Figs. 6D-6F) at different magnifications. The pristine mesh exhibits a typical reticulated structure, with an average wire diameter of approximately 75 µm and pore sizes ranging from 85 to 175 µm. The wire surface appears relatively smooth (Fig. 6C). After ZnO deposition, the overall mesh structure, including wire diameter and pore size, remains largely unchanged (Fig. 6D), indicating that the coating process does not significantly alter the macroscopic geometry of the mesh. However, the wire surface becomes significantly rougher due to the formation of a ZnO layer. At higher magnification, the deposited ZnO structures consist of randomly oriented nanorods and flower-like aggregates distributed across the surface. These hierarchical micro/nanostructures create numerous protrusions and cavities, resulting in a significant increase in surface roughness. Such hierarchical roughness is known to facilitate the trapping of air within the surface structures, promoting the formation of a Cassie-Baxter wetting state when combined with low-surface-energy modification. This structural feature plays a key role in achieving the observed superhydrophobic behaviour.

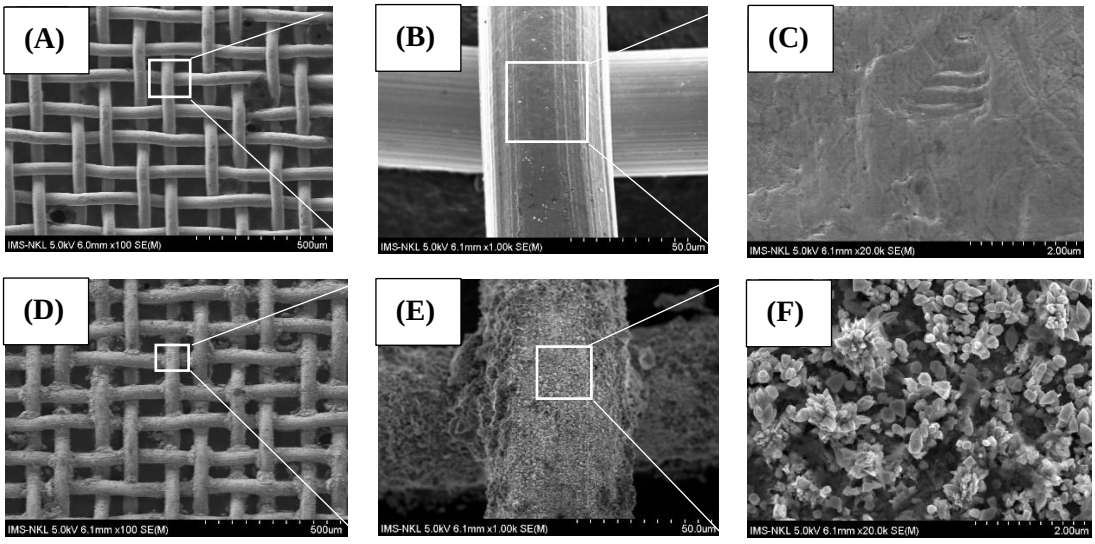


Fig. 6. SEM images of the pristine mesh (A-C) and the superhydrophobic mesh (D-F) at different magnifications. Source: Made by the authors.

The formation of hierarchical ZnO nanorods and flower-like aggregates during electrodeposition follows a nucleation and anisotropic growth mechanism typical of cathodic ZnO electrodeposition from Zn^{2+}-containing baths [29]. At the stainless steel cathode, dissolved oxygen (and, at the applied potential, trace water) is reduced, generating hydroxide ions and raising the local interfacial pH:

$$O_2 + 2H_2O + 4e^- \rightarrow 4OH^- \quad (3)$$

The resulting OH^- reacts with Zn^{2+} supplied by the zinc acetate electrolyte and the sacrificial zinc anode, precipitating $Zn(OH)_2$, which dehydrates to ZnO:

$$Zn^{2+} + 2OH^- \rightarrow Zn(OH)_2 \rightarrow ZnO + H_2O \quad (4)$$

Because OH^- is generated heterogeneously at the electrode surface, ZnO nucleation initiates preferentially at surface defects and wire crossover points, where the local current density is highest. Under the mild, low apparent current conditions employed here (~0.044 mA cm^{-2}), nucleation is followed by anisotropic growth along the polar c-axis of the wurtzite ZnO lattice - the lowest-energy, fastest-growing direction among the low-index facets - yielding elongated one-dimensional nanorods. At longer deposition times, competition between adjacent nucleation sites

and secondary nucleation on the initially formed rods promote branching and radial aggregation, giving rise to the flower-like clusters observed in Figs. 6D-6F.

This nucleation and anisotropic growth pathway accounts for the time-dependent hierarchical roughness observed in this study and underlies the transition from the Wenzel-like wetting state of the pristine mesh to the Cassie-Baxter superhydrophobic state of the ZnO/MTES-modified mesh, as described above.

The surface chemical composition after each modification step was analysed by EDS and FTIR. Fig. 7 compares the FTIR spectra of the pristine, ZnO-coated, and MTES-modified meshes. For the pristine mesh, the broad band at 3240 cm^{-1} corresponds to O-H stretching of adsorbed moisture, and the sharp bands at 525, 499, and 428 cm^{-1} are assigned to Fe-O, Cr-O, and Ni-O vibrations of the native passive oxide film.

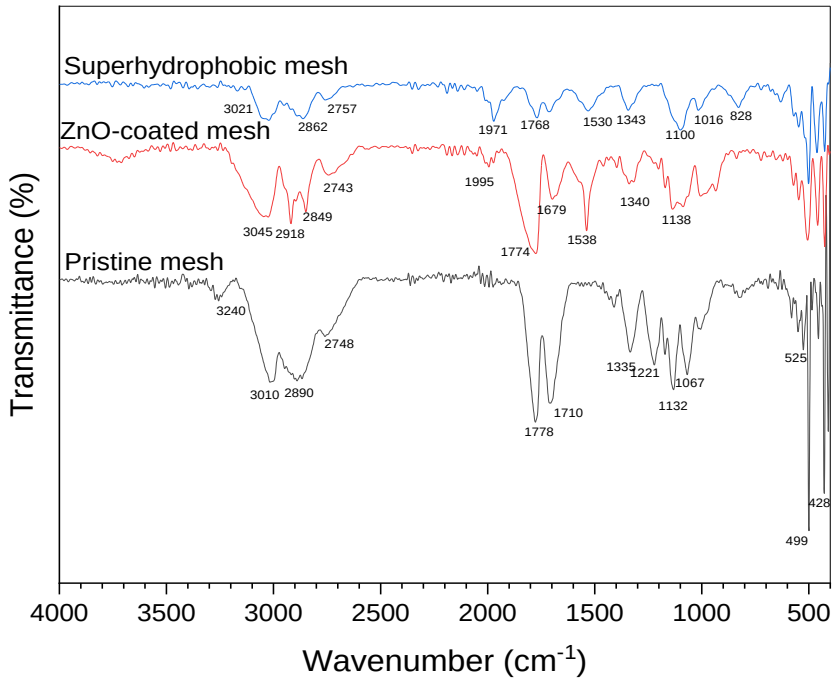


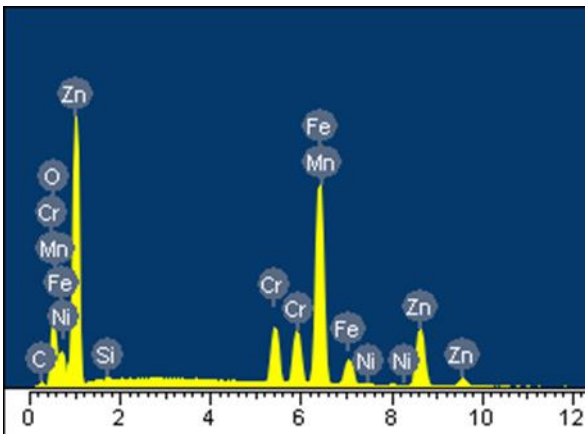
Fig. 7. FTIR spectra of meshes. Source: Made by the authors.

After ZnO electrodeposition, new bands appear at 400-600 cm^{-1}, corresponding to Zn-O stretching vibrations, confirming ZnO formation on the mesh surface, while

residual C-H and COO^- bands (2915-2849 and 1679-1535 cm^{-1}, respectively) indicate trace acetate species retained from the zinc acetate precursor.

Following MTES modification, characteristic bands emerge at 2882 cm^{-1} (C-H stretching of $-CH_3$), 1100-1006 cm^{-1} (Si-O-Si, from silane hydrolysis/condensation), and 828 cm^{-1} (Si-C stretching, $Si-CH_3$ rocking), supporting successful MTES modification and siloxane formation on the ZnO surface. The introduction of low-surface-energy methyl groups, combined with the ZnO-derived hierarchical roughness (SEM, Fig. 6), accounts for the superhydrophobic behaviour of the modified mesh.

The elemental composition of the MTES-modified ZnO-coated mesh was further analysed using EDS (Fig. 8). The spectrum shows Fe as the dominant element, originating from the stainless steel substrate, along with significant Zn and O signals, indicating the presence of a ZnO layer on the mesh surface. The appearance of Si and C signals suggests the successful introduction of the silane modifier on the surface. In addition, the detection of Cr, Mn, and Ni corresponds to the underlying alloy composition of the stainless steel mesh. These results, together with the FTIR and SEM analyses, support the successful surface modification of the mesh through ZnO deposition and subsequent MTES treatment, contributing to the observed superhydrophobic behaviour.



Element	Weight (%)	Atomic (%)
C	**2.58**	**9.13**
O	**10.06**	**26.77**
Si	**0.32**	**0.49**
Cr	7.87	6.44
Mn	8.27	6.41
Fe	40.95	31.21
Ni	0.64	0.47
Zn	**29.31**	**19.08**
Totals	**100.00**	

Fig. 8. EDS results for the superhydrophobic mesh surface. Source: Made by the authors.

3.2. Chemical stability

The chemical stability of the superhydrophobic mesh was evaluated under acidic and alkaline conditions to assess its potential applicability in practical oil/water separation environments. As shown in Fig. 9, the fabricated mesh maintained water contact angles higher than 150° over a broad pH range from 1 to 13, demonstrating stable superhydrophobic behaviour under both acidic and alkaline conditions. This result indicates that the ZnO/MTES-modified mesh can preserve its water-repellent surface over a wide chemical window, which is beneficial for treating oily wastewater with different pH values.

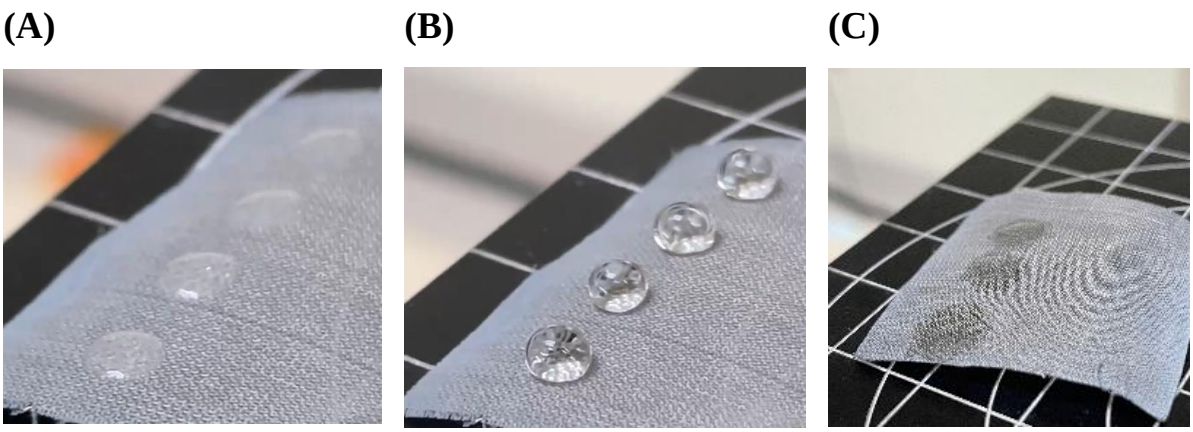


Fig. 9. Photographs of acid and alkaline droplets at different pH values on the superhydrophobic mesh. (A) pH=0 (Hydrophobic); **(B)** 1<pH<13 (Superhydrophobic with CA>150°); **(C)** pH=14 (Hydrophilic). Water contact angle (WCA) values measured by goniometry are superimposed on each panel. Source: Made by the authors.

The loss of superhydrophobicity was observed only under extremely corrosive conditions, namely pH=0 and pH=14, where the water contact angle decreased significantly to approximately 36°. This decrease can be attributed to the deterioration of the surface structure and chemistry under highly aggressive media. The gas evolution observed at pH=0 is attributed to corrosion of the underlying metal substrate, rather than ZnO dissolution. Although ZnO readily dissolves in acidic media according to $ZnO + 2H^+ \rightarrow Zn^{2+} + H_2O$, this reaction produces only dissolved Zn^{2+} and H_2O and therefore cannot account for gas formation. The presence of H_2 bubbles indicates that H^+ ions penetrated through nanoscale pores and defects in the ZnO/MTES coating, particularly at the intersections of the mesh structure where the coating may be thinner, and reached the stainless steel substrate and/or residual metallic Zn. Accordingly, the reaction $M + 2H^+ \rightarrow M^{2+} + H_2\uparrow$ (M = Fe, Zn, Cr, and Ni) is considered the primary mechanism responsible for gas evolution. This behaviour is consistent with a localised Cassie-to-Wenzel transition and acid-induced breakdown of the passive film, promoting H_2 evolution at localised corrosion sites [30]. Overall, the fabricated ZnO/MTES-modified mesh exhibits good chemical stability over a

wide pH range of 1-13, and its superhydrophobicity is compromised only under extremely acidic or alkaline environments. These results suggest that the mesh is suitable for oil/water separation under broad practical conditions, although direct application in highly corrosive media should be avoided.

3.3. Oil/water separation

The modified mesh exhibited strong water repellency and a high affinity for oil, characteristic of a superhydrophobic/superoleophilic (SHB/SOL) surface. As shown in Fig. 10, water droplets maintained an almost spherical shape on the mesh surface, indicating a very high water contact angle, whereas oil droplets spread rapidly upon contact. These observations demonstrate the selective wettability of the modified surface towards oil t”geth’r with its excellent water-repellent behaviour.

Based on these SHB/SOL properties, the fabricated mesh was evaluated using the gravity-driven oil/water separation apparatus and procedure described in Section 2.4 (Figs. 2 and 3). In a representative experiment, the separation process was completed within 50 s, yielding 19.2 ml of collected oil. Using Equations (1) and (2), the corresponding separation efficiency was approximately 96%, with a permeation flux of ~7.82×10^{3} $L\cdot m^{-2}\cdot h^{-1}$, indicating rapid oil transport through the SHB/SOL mesh under gravity-driven conditions. To evaluate the reproducibility of the separation performance, the experiment was independently repeated ten times (n=10), resulting in a mean separation efficiency of 95.7±2.5%.

The reusability of the mesh was further examined over ten consecutive reuse cycles. After each cycle, the mesh was cleaned with ethanol and dried before reuse. The mesh remained functional and maintained its oil/water separation capability throughout the ten-cycle test. However, separation efficiency and permeation flux were not quantitatively recorded for each individual reuse cycle; therefore, the reuse test should be regarded as a qualitative assessment of short-term operational stability rather than a quantitative per-cycle performance evaluation.

The modified mesh also exhibited good storage stability under ambient atmospheric conditions. After six months of storage in air, it retained its superhydrophobic and superoleophilic characteristics, indicating good long-term surface stability. Nevertheless, standardised mechanical durability tests, such as tape peeling, bending, abrasion, and ultrasonic cleaning, were not performed in the present study. Therefore, the current results demonstrate short-term reusability and ambient storage stability, while the resistance of the ZnO/MTES coating to direct mechanical stresses remains to be systematically evaluated in future work.

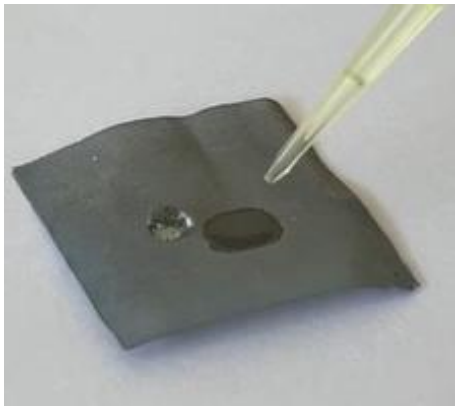


Fig. 10. Water and oil droplets on the superhydrophobic surface. Source: Made by the authors.

Table 2. Comparison of superhydrophobic mesh materials for oil-water separation, including permeation flux and results from this work.

References	Substrate/method	WCA (°)	Separation efficiency (%)	Permeation flux ($L \cdot m^{-2} \cdot h^{-1}$)
[20]	Spray NS/MUF+ODA	>160	>98	not reported
[21]	ZnO nanosheets+STA on SS mesh	162	99 (petrol)/92 (veg. oil)	700±50 (petrol)/135±50 (veg. oil)
[22]	Polystyrene layering	158	>87	not reported
[23]	ZnO/Zn-Ni electrodeposition+PFOTS	—	97.3	6413
[24]	OTS modification	157.5	>89	not reported
[25]	Ni-WS2 coating	169	>98	not reported
This work	ZnO electrodeposition+MTES (fluorine-free)	>150	95.7±2.5	7820

As summarised in Table 2, the ZnO/MTES mesh developed in this work exhibited a representative permeation flux of 7.82×10^3 $L\cdot m^{-2}\cdot h^{-1}$, which is higher than that reported for the electrodeposited ZnO/Zn–Ni/PFOTS mesh in [23] (6413 $L\cdot m^{-2}\cdot h^{-1}$) and the ZnO-nanosheet-coated mesh in [21] (700±50 $L\cdot m^{-2}\cdot h^{-1}$ for petrol). Although the mean separation efficiency obtained in this work (95.7±2.5%, n=10) is slightly lower than several reported efficiencies exceeding 98%, it demonstrates good and reproducible separation performance using a fluorine-free MTES modifier. Overall, these results indicate that the ZnO/MTES mesh provides competitive gravity-driven oil/water separation performance, particularly in terms of permeation flux, while avoiding the use of fluorinated surface modifiers.

It is acknowledged that several superhydrophobic mesh materials reported between 2024 and 2026 achieve separation efficiencies exceeding 98-99% [21, 25], whereas the present work reports a mean efficiency of 95.7±2.5%. We attribute this gap primarily to methodological factors in the separation apparatus and protocol rather than to a limitation of the intrinsic wettability of the ZnO/MTES surface (WCA>150°, complete oil wetting; Fig. 10). Specifically, (i) a small residual film of oil remains adhered to the wall of the open-top loading tube above the mesh (Fig. 2) and is not credited towards the permeated volume in Equation (1), even though it never contacted the mesh surface, and (ii) the short, single gravity-driven pass used here, without a post-separation drainage step, limits the time available for the last few millilitres of oil to fully permeate. Apparatus reported to achieve >98% efficiency typically employ a larger mesh working area relative to the charged liquid volume, an extended drainage/settling period, or suction/vacuum assistance, rather than a fundamentally different surface chemistry. This indicates that the ~96% efficiency reflects the specific apparatus/protocol used for this initial-stage feasibility study rather than an intrinsic ceiling of the ZnO/MTES coating itself, and we report it transparently as such rather than as a re-optimised value.

4. Conclusions

A fluorine-free superhydrophobic/superoleophilic stainless steel mesh was fabricated by ZnO electrodeposition followed by MTES modification, achieving a water contact angle above 150°, a mean oil/water separation efficiency of 95.7±2.5% (n=10), and a representative permeation flux of 7.82×10^3 $L\cdot m^{-2}\cdot h^{-1}$.

The mesh maintained superhydrophobicity over a pH range of 1-13 and after six months of ambient storage, while remaining functional over ten consecutive reuse cycles. These results demonstrate good chemical stability, short-term reusability, and storage stability of the ZnO/MTES-modified mesh. The combination of ZnO electrodeposition and fluorine-free MTES modification therefore provides a simple and effective route for preparing superhydrophobic stainless steel meshes for gravity-driven oil/water separation.

CRediT author statement

Nguyen Thi Phuong Nhung: Literature review, Conceptualisation, Data analysis, Conducting experiments, Writing, Reviewing and Editing; Vo Chi Hao: Conducting experiments.

ACKNOWLEDGEMENTS

The current project was financially supported by PetroVietnam University under grant code GV2406.

COMPETING INTERESTS

The authors declare that there is no conflict of interest regarding the publication of this article.

REFERENCES

[1] N.Y. Abu-Thabit, M.H. Abu Elella, A.K. Azad, et al. (2025), “Superwetting metal mesh membranes for oil/water separation: A comprehensive review”, *Separation and Purification Technology*, **363**, DOI: 10.1016/j.seppur.2025.132016.

[2] N.T.P. Nhung, N.T.N. Tien, N.H. Luong, et al. (2022), “Micro/nanostructured ZnO-based superhydrophobic steel surface with enhanced corrosion protection”, *PetroVietnam Journal*, **6**, pp.59-66, DOI:

10.47800/PVJ.2022.06-07.

[3] G.D. Patil, A.H. Patil, S.A. Jadhav, et al. (2019), "A new method to prepare superhydrophobic cotton fabrics by postcoating surface modification of ZnO nanoparticles", *Materials Letters*, **255**, DOI: 10.1016/j.matlet.2019.126562.

[4] T.P.N. Nguyen, M.Q.B. Phan, V.T. Huynh (2024a), "Facile fabrication of superhydrophobic ZnO powders coated on polyurethane sponge for effective oil/water separation application", *Vietnam Journal of Catalysis and Adsorption*, **13(2)**, pp.123-128, DOI: 10.62239/jca.2024.043.

[5] S. Gupta, N.H. Tai (2016), "Carbon materials as oil sorbents: A review on the synthesis and performance", *Journal of Materials Chemistry A*, **4(5)**, pp.1550-1565, DOI: 10.1039/c5ta08321d.

[6] S.S. Latthe, R.S. Sutar, A.K. Bhosale, et al. (2019), "Chapter 15 - Superhydrophobic surfaces for oil-water separation", *Superhydrophobic Polymer Coatings: Fundamentals, Design, Fabrication, and Applications*, Elsevier, pp.339-356, DOI: 10.1016/B978-0-12-816671-0.00016-3.

[7] T.P.N. Nguyen, T.T. Phan, Q.V. Dang, et al. (2024b), "Fabrication of a superhydrophobic RGO coated-polyurethan sponge for removing oil, organic solvent, and gasoline from water", *Journal of Technical Education Science*, **19(5)**, pp.67-73, DOI: 10.54644/jte.2024.1573.

[8] A.K. Azad, N.Y. Abu-Thabit, M.H. Abu Elella (2025), "Sustainable and durable superwetting textiles coated with polydopamine for oil/water separation", *RSC Sustainability*, **3(6)**, pp.2501-2533, DOI: 10.1039/d5su00041f.

[9] Y. Li, Z. Han, M. Gao, et al. (2023), "Bioinspired and green fabrication of superhydrophobic materials with good robustness, stability and flame retardancy for oil-water separation based on waste cotton", *Industrial Crops and Products*, **206**, DOI: 10.1016/j.indcrop.2023.117591.

[10] Z. Han, X. Lv, Y. Li, et al. (2025), "Biomimetic design and construction of biobased, superhydrophobic and multifunctionality-integration cotton fabrics for efficient oil/water separation", *Journal of Environmental Chemical Engineering*, **13(4)**, DOI: 10.1016/j.jece.2025.117116.

[11] C. Liao, Y. Li, M. Gao, et al. (2022), "Bio-inspired construction of super-hydrophobic, eco-friendly multifunctional and bio-based cotton fabrics via impregnation method", *Colloids and Surfaces A: Physicochemical and Engineering Aspects*, **651**, DOI: 10.1016/j.colsurfa.2022.129647.

[12] C. Liao, Y. Li, M. Gao, et al. (2023), "Bio-inspired and facile fabrication strategy of biobased, halogen-free and superhydrophobic cotton fabrics with multifunctionality and durability", *Colloids and Surfaces A: Physicochemical and Engineering Aspects*, **657**, DOI: 10.1016/j.colsurfa.2022.130586.

[13] X. Lv, Y. Song, Z. Han, et al. (2025), "Bio-inspired, recycled and durable construction of superhydrophobic/oleophilic cotton fabrics with excellent oil/water separation ability based on dual carbon materials", *Process Safety and Environmental Protection*, **201**, DOI: 10.1016/j.psep.2025.107504.

[14] C. Liao, Y. Xia, A.Y.N. Keshen, et al. (2021), "A facile and green construction of biomimetic, fluorine-free and superhydrophobic melamine sponge with magnetic-driven function for efficient oil-water separation and oil absorption", *Journal of Bionic Engineering*, **18(5)**, pp.1168-1178, DOI: 10.1007/s42235-021-00078-9.

[15] Z. Han, X. Lv, Y. Li, et al. (2024), "Preparation of superhydrophobic and multifunctional sponges for oil/water separation and oil absorption", *Langmuir*, **40(45)**, pp.23902-23917, DOI: 10.1021/acs.langmuir.4c03036.

[16] M. Zhu, Y. Liu, M. Chen, et al. (2021), "Metal mesh-based special wettability materials for oil-water separation: A review of the recent development", *Journal of Petroleum Science and Engineering*, **205**, DOI: 10.1016/j.petrol.2021.108889.

[17] H. Shayesteh, R. Norouzbeigi, A. Rahbar-Kelishami (2022a), "Evaluation of superhydrophobicity of chemical-resistant magnetic spiky nickel nanowires grafted with silane coupling agent for highly efficient oil/water separation", *Surfaces and Interfaces*, **28**, DOI: 10.1016/j.surfin.2021.101685.

[18] H. Shayesteh, A. Rahbar-Kelishami, R. Norouzbeigi (2022b), "Superhydrophobic/superoleophilic micro/nanostructure nickel particles for

oil/water mixture and emulsion separation", *Ceramics International*, **48(8)**, pp.10999-11008, DOI: 10.1016/j.ceramint.2021.12.320.

[19] J.T. Simpson, S.R. Hunter, T. Aytug (2015), "Superhydrophobic materials and coatings: A review", *Reports on Progress in Physics*, **78(8)**, DOI: 10.1088/0034-4885/78/8/086501.

[20] L. Kang, X. Dang, F. Li, et al. (2026), "Fabrication of superhydrophobic stainless steel mesh with hierarchical micro-nano structures for oil/water separation", *Surfaces and Interfaces*, **87**, DOI: 10.1016/j.surfin.2026.108898.

[21] T.A. Ekunde, P.P. Gaikwad, R.S. Sutar, et al. (2025), "Superhydrophobic northern tooth-like ZnO nanosheets on stainless steel mesh for oil-water separation", *Journal of Water Process Engineering*, **71**, DOI: 10.1016/j.jwpe.2025.107368.

[22] R.S. Sutar, S.S. Latthe, A.R. Jundle, et al. (2024), "A facile approach for oil-water separation using superhydrophobic polystyrene-silica coated stainless steel mesh bucket", *Marine Pollution Bulletin*, **198**, DOI: 10.1016/j.marpolbul.2023.115790.

[23] H. Xiang, W. Zhang, X. Huang, et al. (2025), "ZnO nanoparticle-enhanced Zn/Ni superhydrophobic stainless steel mesh: Microstructural control for high-efficiency oil-water separation", *Journal of Environmental Chemical Engineering*, **13(5)**, DOI: 10.1016/j.jece.2025.117595.

[24] R.S. Sutar, S.S. Latthe, N.B. Gharge, et al. (2023), "Facile approach to fabricate a high-performance superhydrophobic PS/OTS modified SS mesh for oil-water separation", *Colloids and Surfaces A: Physicochemical and Engineering Aspects*, **657**, DOI: 10.1016/j.colsurfa.2022.130561.

[25] R. Sreekumar, S.E. Thazhakkuni, S.S. Suseelamma (2024), "Fabrication of a robust superhydrophobic stainless steel mesh for efficient oil/water separation", *Journal of Industrial and Engineering Chemistry*, **135**, pp.425-433, DOI: 10.1016/j.jiec.2024.01.054.

[26] C. Wang, T. Yao, J. Wu, et al. (2009), "Facile approach in fabricating superhydrophobic and superoleophilic surface for water and oil mixture

separation", *ACS Applied Materials and Interfaces*, **1(11)**, pp.2613-2617, DOI: 10.1021/am900520z.

[27] Y. Cheng, B. Wu, X. Ma, et al. (2018), "Facile preparation of high density polyethylene superhydrophobic/superoleophilic coatings on glass, copper and polyurethane sponge for self-cleaning, corrosion resistance and efficient oil/water separation", *Journal of Colloid and Interface Science*, **525**, pp.76-85, DOI: 10.1016/j.jcis.2018.04.075.

[28] A. Deachophon, T. Bovornratanaraks, S. Poompradub (2024), "Modified silica-based double-layered hydrophobic-coated stainless steel mesh and its application for oil/seawater separation", *Scientific Reports*, **14**, DOI: 10.1038/s41598-024-51264-8.

[29] M. Kumar, C. Sasikumar (2014), "Electrodeposition of nanostructured ZnO thin film: A review", *American Journal of Materials Science and Engineering*, **2(2)**, pp.18-23, DOI: 10.12691/ajmse-2-2-2.

[30] S. Choudhary, R.G. Kelly, N. Birbilis (2024), "On the origin of passive film breakdown and metastable pitting for stainless steel 316L", *Corrosion Science*, **230**, DOI: 10.1016/j.corsci.2024.111911.